

A Multi-Resolution Approach for *BCS*-Based Imaging of Sparse Scatterers

N. Anselmi, L. Poli, G. Oliveri, and A. Massa

Abstract

In this work, a novel Bayesian compressive sensing (*BCS*)-based microwave imaging method is proposed. The developed technique suitably combines the regularization properties of *CS* techniques with those of the iterative multi-scale approach (*IMSA*), in order to exploit the progressively acquired information on the scatterer location and size and improve the overall accuracy of the retrieved images. Toward this end, an innovative information-driven relevance vector machine (*RVM*) has been developed. Some preliminary results are shown to verify the effectiveness of the proposed *IMSA-BCS* strategy.

1 Mathematical Formulation

Let us consider an inaccessible investigation domain Λ irradiated by a set of incident transverse-magnetic planes $E_{inc}^v(\mathbf{r}^v)$, $v = 1, \dots, V$, impinging from the angular directions $\theta^v = \frac{2\pi}{V}(v - 1)$, being V the number of views.

In this working scenario, the scattered field $E_{scatt}^v(\mathbf{r}_s^v)$, $s = 1, \dots, S$, is supposed to be measured through a set of S sensors equally displaced on a circular observation domain Θ , external to the investigation domain ($\Lambda \cap \Theta = 0$), having radius ρ . The exact location of the sensors are identified by the position vector $\mathbf{r}_s^v = (\rho \cos \theta_s^v \sin \theta_s^v)$, being $\theta_s^v = \theta^v + \frac{2\pi}{S}(s - 1)$.

This scattered field is known to be dependent on the equivalent currents $J_{eq}^v(\mathbf{r})$ generated in the support of the unknown scatterers placed into the domain Λ , according to the *data equation*

$$E_{scatt}^v(\mathbf{r}_s^v) = -k_0^2 \int_{\Lambda} J_{eq}^v(\mathbf{r}') G(\mathbf{r}_s^v / \mathbf{r}') \quad (1)$$

where $G(\mathbf{r}_s^v / \mathbf{r}')$ is the Green's function in the free space and $k_0 = \omega \sqrt{\epsilon_0 \mu_0}$. The material properties of the investigation domain Λ in terms of relative dielectric permittivity $\epsilon_r(\mathbf{r})$ and electric conductivity $\sigma(\mathbf{r})$ are described by means of the object function

$$\tau(\mathbf{r}) = \epsilon_r(\mathbf{r}) - \epsilon_0 - \frac{\sigma(\mathbf{r})}{2\pi f \epsilon_0} \quad (2)$$

f being the frequency of the TM plane wave.

In order to numerically deal with (1), the investigation domain is discretized into N sub-domains (cells), providing the matrix form of

$$\mathbf{E}^v = \mathbf{G} \mathbf{J}_{eq}^v + \mathbf{N}^v \quad (3)$$

\mathbf{G} being the Green's matrix and \mathbf{N}^v a zero mean additive Gaussian noise vector of variance σ^2 . The dielectric features of the N sub-domains described through the discretized form of the object function τ are then retrieved through the following iterative strategy which combines a multi-resolution approach and the *BCS* method, aimed to maximize the a-posteriori probability of the equivalent sources given the scattered field as:

$$\hat{\mathbf{J}}_{eq}^v = \arg \left\{ \max \left[\mathcal{P} \left(\mathbf{J}_{eq}^v | \mathbf{E}_{scatt}^v \right) \right] \right\}, \quad v = 1, \dots, V \quad (4)$$

More in detail, the algorithms works as follows:

1. *Initialization*: Definition of input parameters of the *BCS* problem, namely the initial estimation of the noise on the scattered data, σ_{init}^2 , the convergence parameter, γ , and the parameter related to the stopping criterion of the *IMSA*, χ . Set the region of interest equal to the whole domain $\mathcal{D}^{(1)} = \Lambda$;
2. *BCS inversion via “Constrained-RVM”*:
 - (a) increase of the iteration index: $i = i + 1$;
 - (b) solution of the *BCS* problem within the Region of Interest (*RoI*) $\mathcal{D}^{(i-1)}$ defined at the $(i-1)$ -th step,

by maximizing the following cost function:

$$\ell(\mathbf{a}^v) = -0.5 \left[2S \log(2\pi) + \log(\mathbf{C}) + (\mathbf{E}_{scatt}^v)^T \mathbf{C}^{-1} (\mathbf{E}_{scatt}^v) \right], \quad v = 1, \dots, V \quad (5)$$

where $\mathbf{C} = \sigma^2 \mathbf{I} + \mathbf{G} [diag(\mathbf{a}^v)]^{-1} \mathbf{G}^T$ and being \mathbf{a}^v the hyperparameter vector whose entries corresponding to the cells out of the *RoI* $\mathcal{D}^{(i-1)}$ are forced to ∞ ;

3. Equivalent Current Retrieval:

Computation of the equivalent currents starting from the hyperparameter vector \mathbf{a}^v according to:

$$\mathbf{J}_{eq}^v = \frac{1}{\sigma^2} \left[\frac{\mathbf{G}^T \mathbf{G}}{\sigma^2} diag(\mathbf{a}^v) \right]^{-1} \mathbf{G}^T \mathbf{E}_{scatt}^v, \quad v = 1, \dots, V \quad (6)$$

4. Features' Retrieval:

Reconstruction of the material properties of the investigation domain taking advantage from the first order Born approximation through

$$\tau(\mathbf{r}_n^{(i)}) = \frac{1}{V} \sum \frac{\mathbf{J}_{eq}^v(\mathbf{r}_n^{(i)})}{\mathbf{E}_{inc}^v(\mathbf{r}_n^{(i)})}, \quad n = 1, \dots, N \quad (7)$$

being $\mathbf{r}_n^{(i)}$ the barycenter of the n-th cell within the *RoI* $\mathcal{D}^{(i-1)}$;

5. Convergence Check:

Definition of the new *RoI* $\mathcal{D}^{(i)}$ according to the contrast function distribution and evaluation of the following termination condition:

$$\left(\frac{L^{(i-1)} - L^{(i)}}{L^{(i)}} \right) < \chi \quad (8)$$

being $L^{(i)}$ the side of the *RoI* $\mathcal{D}^{(i)}$. If such a condition is met, then stop the iterative process, otherwise go to step 2.

2 Preliminary Numerical Assessment

2.1 L-shaped Object, $\ell = 1.5\lambda$

Test Case Description

Direct solver:

- Side of the investigation domain: $L = 6.0\lambda$
- Cubic domain divided in $\sqrt{D} \times \sqrt{D}$ cells
- Number of cells for the direct solver: $D = 1600$ (discretization = $\lambda/10$)

Investigation domain:

- Cubic domain divided in $\sqrt{N} \times \sqrt{N}$ cells
- Number of cells for the inversion:
 - First Step IMSA: $N^{(1)} = 100$ (discretization = $\lambda/10$)
 - Following Steps IMSA: $N^{(i)}$ not fixed, defined according to the estimated *RoI* $\mathcal{D}^{(i)}$

Measurement domain:

- Total number of measurements: $M = 60$
- Measurement points placed on circles of radius $\rho = 4.5\lambda$

Sources:

- Plane waves
- Number of views: $V = 60$; $\theta_{inc}^v = 0^\circ + (v - 1) \times (360/V)$
- Amplitude: $A = 1.0$
- Frequency: $F = 300$ MHz ($\lambda = 1$)

Background:

- $\epsilon_r = 1.0$
- $\sigma = 0$ [S/m]

Scatterer

- L-shaped object, $\ell = 1.5\lambda$
- $\epsilon_r \in \{1.01, 1.02, 1.04, 1.05, 1.06, 1.08, 1.10, 1.15, 1.20\}$
- $\sigma = 0$ [S/m]

2.1.1 L-shaped Object, $\ell = 1.5\lambda$, $\tau = 0.02$ - IMSA-BCS reconstructed profiles

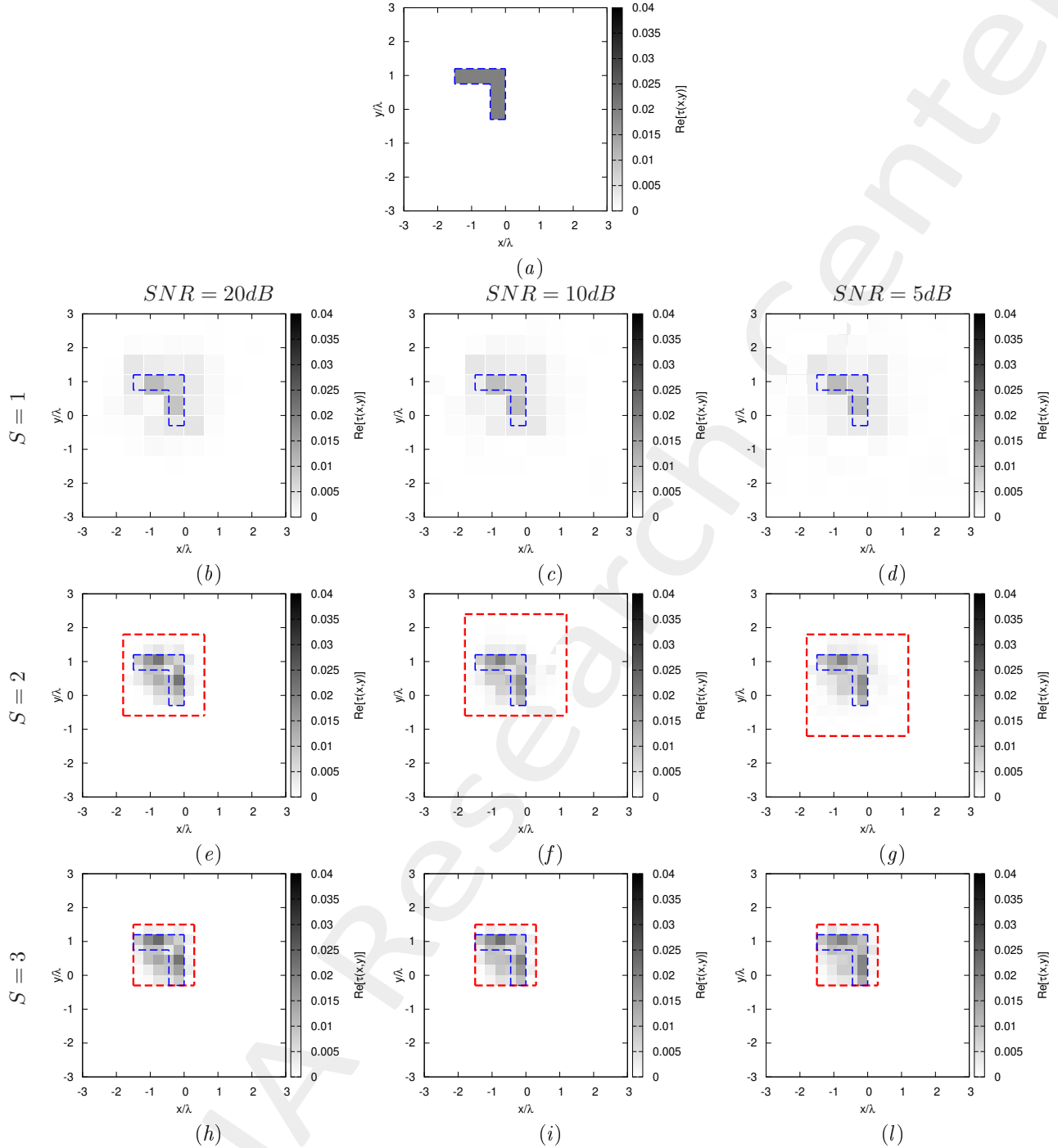


Figure 1: *L-shaped Object, $\ell = 1.5\lambda$, $\tau = 0.02$* - (a) Actual profile and (b)-(o) IMSA-BCS reconstructed profiles for (b)(e)(h) $SNR = 20$ [dB], (c)(f)(i) $SNR = 10$ [dB] and (d)(g)(l) $SNR = 5$ [dB] at the step (b)-(d) $S = 1$, (e)-(g) $S = 2$, and (h)-(l) $S = 3$.

| | $SNR = 50dB$ | | | |
|-------------|-----------------------|-----------------------|-----------------------|-----------------------|
| | $S = 1$ | $S = 2$ | $S = 3$ | $S = 4$ |
| ξ_{tot} | 9.01×10^{-4} | 5.09×10^{-4} | 5.64×10^{-4} | 5.64×10^{-4} |
| ξ_{int} | 1.20×10^{-2} | 8.97×10^{-3} | 1.04×10^{-2} | 1.04×10^{-2} |
| ξ_{ext} | 5.30×10^{-4} | 2.29×10^{-4} | 2.39×10^{-4} | 2.39×10^{-4} |
| | $SNR = 20dB$ | | | |
| | $S = 1$ | $S = 2$ | $S = 3$ | $S = 4$ |
| ξ_{tot} | 9.09×10^{-4} | 5.21×10^{-4} | 4.85×10^{-4} | 5.72×10^{-4} |
| ξ_{int} | 1.21×10^{-2} | 9.18×10^{-3} | 8.73×10^{-3} | 1.04×10^{-2} |
| ξ_{ext} | 5.34×10^{-4} | 2.35×10^{-4} | 2.13×10^{-4} | 2.47×10^{-4} |
| | $SNR = 10dB$ | | | |
| | $S = 1$ | $S = 2$ | $S = 3$ | $S = 4$ |
| ξ_{tot} | 9.38×10^{-4} | 5.18×10^{-4} | 4.69×10^{-4} | 5.42×10^{-4} |
| ξ_{int} | 1.22×10^{-2} | 8.85×10^{-3} | 8.26×10^{-3} | 1.01×10^{-2} |
| ξ_{ext} | 5.56×10^{-4} | 2.42×10^{-4} | 2.12×10^{-4} | 2.24×10^{-4} |
| | $SNR = 5dB$ | | | |
| | $S = 1$ | $S = 2$ | $S = 3$ | $S = 4$ |
| ξ_{tot} | 9.73×10^{-4} | 5.31×10^{-4} | 4.34×10^{-4} | 4.34×10^{-4} |
| ξ_{int} | 1.22×10^{-2} | 8.84×10^{-3} | 7.44×10^{-3} | 7.44×10^{-3} |
| ξ_{ext} | 5.85×10^{-4} | 2.50×10^{-4} | 2.01×10^{-4} | 2.01×10^{-4} |

Table I: *L-shaped Object*, $\ell = 1.5\lambda$, $\tau = 0.02$ - Reconstruction errors: total (ξ_{tot}), internal (ξ_{int}) and external (ξ_{ext}) errors.

| | $SNR = 50dB$ | | | |
|-----------|--------------|---------|---------|---------|
| | $S = 1$ | $S = 2$ | $S = 3$ | $S = 4$ |
| $L^{(S)}$ | 6.00 | 1.50 | 1.50 | 1.50 |
| $N^{(S)}$ | 100 | 148 | 148 | 148 |
| $Q^{(S)}$ | 100 | 64 | 25 | 25 |
| | $SNR = 20dB$ | | | |
| | $S = 1$ | $S = 2$ | $S = 3$ | $S = 4$ |
| $L^{(S)}$ | 6.00 | 1.50 | 1.50 | 1.50 |
| $N^{(S)}$ | 100 | 148 | 148 | 148 |
| $Q^{(S)}$ | 100 | 64 | 36 | 25 |
| | $SNR = 10dB$ | | | |
| | $S = 1$ | $S = 2$ | $S = 3$ | $S = 4$ |
| $L^{(S)}$ | 6.00 | 1.50 | 1.50 | 1.50 |
| $N^{(S)}$ | 100 | 175 | 175 | 175 |
| $Q^{(S)}$ | 100 | 100 | 36 | 25 |
| | $SNR = 5dB$ | | | |
| | $S = 1$ | $S = 2$ | $S = 3$ | $S = 4$ |
| $L^{(S)}$ | 6.00 | 1.80 | 1.80 | 1.80 |
| $N^{(S)}$ | 100 | 175 | 175 | 175 |
| $Q^{(S)}$ | 100 | 100 | 36 | 36 |

Table II: *L-shaped Object*, $\ell = 1.5\lambda$, $\tau = 0.02$ - Investigation domain parameters: restricted investigation domain size $L^{(S)}$, total number of cells $N^{(S)}$ and number of cells within the restricted domain size $Q^{(S)}$.

2.1.2 L-shaped Object, $\ell = 1.5\lambda$, $\tau = 0.05$ - IMSA-BCS reconstructed profiles

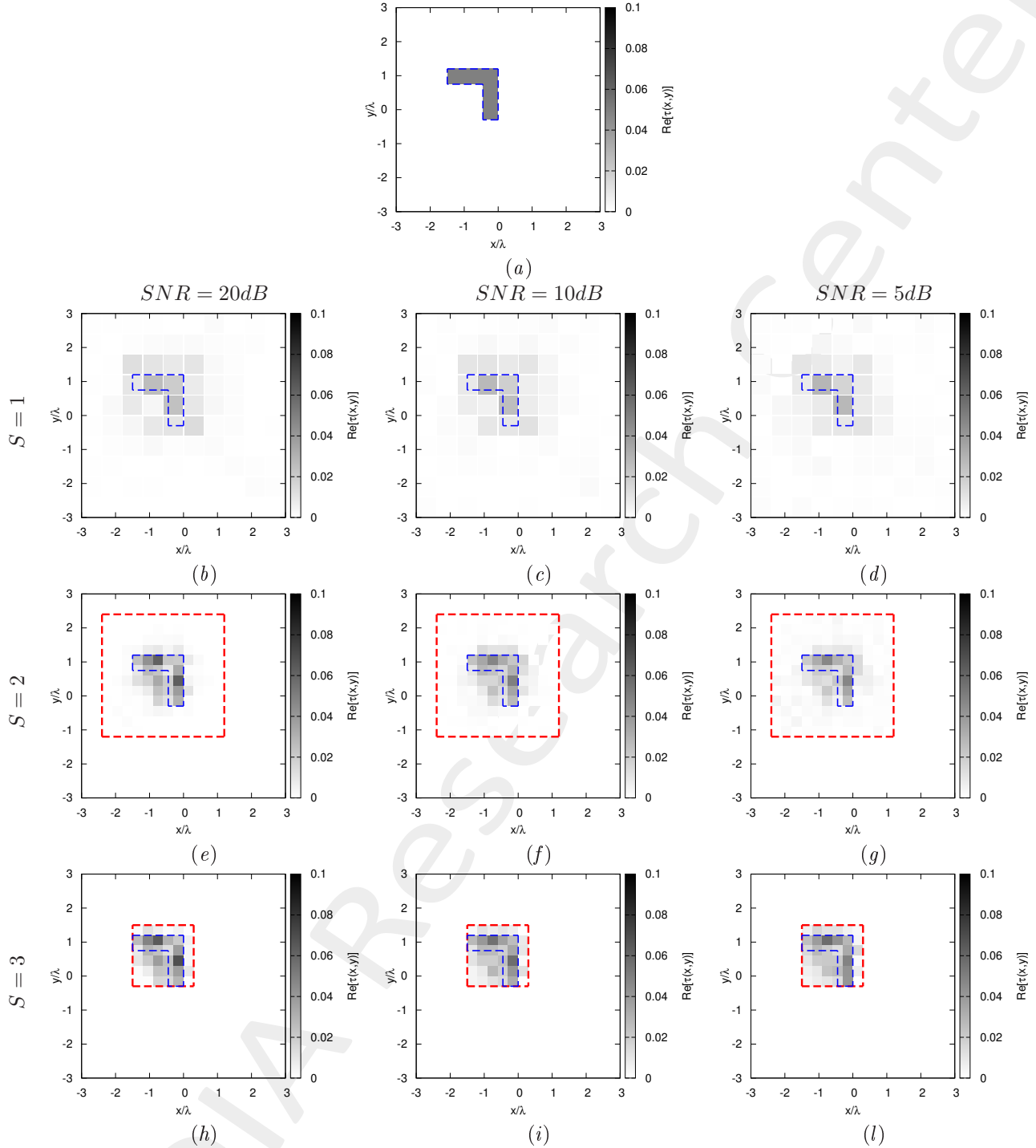


Figure 2: *L-shaped Object, $\ell = 1.5\lambda$, $\tau = 0.05$* - (a) Actual profile and (b)-(o) IMSA-BCS reconstructed profiles for (b)(e)(h) $SNR = 20$ [dB], (c)(f)(i) $SNR = 10$ [dB] and (d)(g)(l) $SNR = 5$ [dB] at the step (b)-(d) $S = 1$, (e)-(g) $S = 2$, and (h)-(l) $S = 3$.

| | $SNR = 50dB$ | | | |
|-------------|-----------------------|-----------------------|-----------------------|-----------------------|
| | $S = 1$ | $S = 2$ | $S = 3$ | $S = 4$ |
| ξ_{tot} | 2.75×10^{-3} | 1.31×10^{-3} | 1.23×10^{-3} | 1.23×10^{-3} |
| ξ_{int} | 2.82×10^{-2} | 2.00×10^{-2} | 1.99×10^{-2} | 1.99×10^{-2} |
| ξ_{ext} | 1.87×10^{-3} | 6.78×10^{-4} | 6.12×10^{-4} | 6.12×10^{-4} |
| | $SNR = 20dB$ | | | |
| | $S = 1$ | $S = 2$ | $S = 3$ | $S = 4$ |
| ξ_{tot} | 2.77×10^{-3} | 1.39×10^{-3} | 1.23×10^{-3} | 1.23×10^{-3} |
| ξ_{int} | 2.84×10^{-2} | 2.14×10^{-2} | 1.98×10^{-2} | 1.98×10^{-2} |
| ξ_{ext} | 1.86×10^{-3} | 7.21×10^{-4} | 6.17×10^{-4} | 6.17×10^{-4} |
| | $SNR = 10dB$ | | | |
| | $S = 1$ | $S = 2$ | $S = 3$ | $S = 4$ |
| ξ_{tot} | 2.81×10^{-3} | 1.47×10^{-3} | 1.19×10^{-3} | 1.19×10^{-3} |
| ξ_{int} | 2.83×10^{-2} | 1.98×10^{-2} | 1.74×10^{-2} | 1.74×10^{-2} |
| ξ_{ext} | 1.87×10^{-3} | 8.23×10^{-4} | 6.50×10^{-4} | 6.50×10^{-4} |
| | $SNR = 5dB$ | | | |
| | $S = 1$ | $S = 2$ | $S = 3$ | $S = 4$ |
| ξ_{tot} | 2.93×10^{-3} | 1.67×10^{-3} | 1.19×10^{-3} | 1.19×10^{-3} |
| ξ_{int} | 2.82×10^{-2} | 2.20×10^{-2} | 1.66×10^{-2} | 1.66×10^{-2} |
| ξ_{ext} | 1.98×10^{-3} | 9.33×10^{-4} | 6.73×10^{-4} | 6.73×10^{-4} |

Table III: *L-shaped Object*, $\ell = 1.5\lambda$, $\tau = 0.05$ - Reconstruction errors: total (ξ_{tot}), internal (ξ_{int}) and external (ξ_{ext}) errors.

| | $SNR = 50dB$ | | | |
|-----------|--------------|---------|---------|---------|
| | $S = 1$ | $S = 2$ | $S = 3$ | $S = 4$ |
| $L^{(S)}$ | 6.00 | 1.80 | 1.80 | 1.80 |
| $N^{(S)}$ | 100 | 208 | 208 | 208 |
| $Q^{(S)}$ | 100 | 144 | 36 | 36 |
| | $SNR = 20dB$ | | | |
| | $S = 1$ | $S = 2$ | $S = 3$ | $S = 4$ |
| $L^{(S)}$ | 6.00 | 1.80 | 1.80 | 1.80 |
| $N^{(S)}$ | 100 | 208 | 208 | 208 |
| $Q^{(S)}$ | 100 | 144 | 36 | 36 |
| | $SNR = 10dB$ | | | |
| | $S = 1$ | $S = 2$ | $S = 3$ | $S = 4$ |
| $L^{(S)}$ | 6.00 | 1.80 | 1.80 | 1.80 |
| $N^{(S)}$ | 100 | 208 | 208 | 208 |
| $Q^{(S)}$ | 100 | 144 | 36 | 36 |
| | $SNR = 5dB$ | | | |
| | $S = 1$ | $S = 2$ | $S = 3$ | $S = 4$ |
| $L^{(S)}$ | 6.00 | 1.80 | 1.80 | 1.80 |
| $N^{(S)}$ | 100 | 208 | 208 | 208 |
| $Q^{(S)}$ | 100 | 144 | 36 | 36 |

Table IV: *L-shaped Object*, $\ell = 1.5\lambda$, $\tau = 0.05$ - Investigation domain parameters: restricted investigation domain size $L^{(S)}$, total number of cells $N^{(S)}$ and number of cells within the restricted domain size $Q^{(S)}$.

2.1.3 L-shaped Object, $\ell = 1.5\lambda$, $\tau = 0.10$ - IMSA-BCS reconstructed profiles

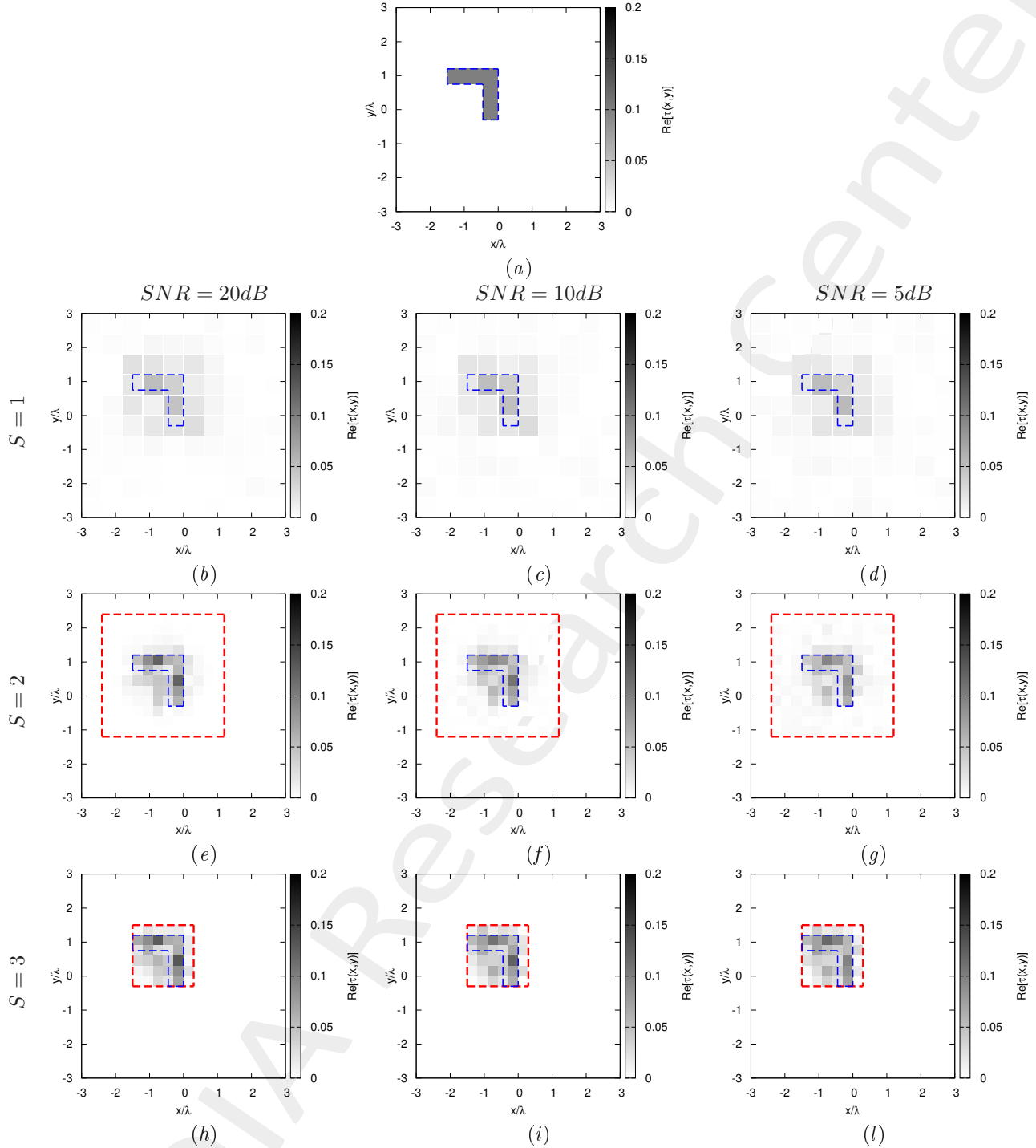


Figure 3: *L-shaped Object, $\ell = 1.5\lambda$, $\tau = 0.10$* - (a) Actual profile and (b)-(o) IMSA-BCS reconstructed profiles for (b)(e)(h) $\text{SNR} = 20$ [dB], (c)(f)(i) $\text{SNR} = 10$ [dB] and (d)(g)(l) $\text{SNR} = 5$ [dB] at the step (b)-(d) $S = 1$, (e)-(g) $S = 2$, and (h)-(l) $S = 3$.

| | $SNR = 50dB$ | | | |
|-------------|-----------------------|-----------------------|-----------------------|-----------------------|
| | $S = 1$ | $S = 2$ | $S = 3$ | $S = 4$ |
| ξ_{tot} | 5.91×10^{-3} | 2.63×10^{-3} | 2.36×10^{-3} | 2.36×10^{-3} |
| ξ_{int} | 5.53×10^{-2} | 3.67×10^{-2} | 3.50×10^{-2} | 3.50×10^{-2} |
| ξ_{ext} | 4.05×10^{-3} | 1.40×10^{-3} | 1.21×10^{-3} | 1.21×10^{-3} |
| | $SNR = 20dB$ | | | |
| | $S = 1$ | $S = 2$ | $S = 3$ | $S = 4$ |
| ξ_{tot} | 5.89×10^{-3} | 2.85×10^{-3} | 2.42×10^{-3} | 2.42×10^{-3} |
| ξ_{int} | 5.55×10^{-2} | 3.99×10^{-2} | 3.57×10^{-2} | 3.57×10^{-2} |
| ξ_{ext} | 4.03×10^{-3} | 1.51×10^{-3} | 1.25×10^{-3} | 1.25×10^{-3} |
| | $SNR = 10dB$ | | | |
| | $S = 1$ | $S = 2$ | $S = 3$ | $S = 4$ |
| ξ_{tot} | 5.97×10^{-3} | 2.91×10^{-3} | 2.55×10^{-3} | 2.55×10^{-3} |
| ξ_{int} | 5.49×10^{-2} | 3.67×10^{-2} | 3.55×10^{-2} | 3.55×10^{-2} |
| ξ_{ext} | 4.06×10^{-3} | 1.64×10^{-3} | 1.39×10^{-3} | 1.39×10^{-3} |
| | $SNR = 5dB$ | | | |
| | $S = 1$ | $S = 2$ | $S = 3$ | $S = 4$ |
| ξ_{tot} | 6.34×10^{-3} | 3.91×10^{-3} | 2.47×10^{-3} | 2.47×10^{-3} |
| ξ_{int} | 5.49×10^{-2} | $Nan \times 10^{-a}$ | 3.22×10^{-2} | 3.22×10^{-2} |
| ξ_{ext} | 4.22×10^{-3} | 3.66×10^{-3} | 1.36×10^{-3} | 1.36×10^{-3} |

Table V: *L-shaped Object*, $\ell = 1.5\lambda$, $\tau = 0.10$ - Reconstruction errors: total (ξ_{tot}), internal (ξ_{int}) and external (ξ_{ext}) errors.

| | $SNR = 50dB$ | | | |
|-----------|--------------|---------|---------|---------|
| | $S = 1$ | $S = 2$ | $S = 3$ | $S = 4$ |
| $L^{(S)}$ | 6.00 | 1.80 | 1.80 | 1.80 |
| $N^{(S)}$ | 100 | 208 | 208 | 208 |
| $Q^{(S)}$ | 100 | 144 | 36 | 36 |
| | $SNR = 20dB$ | | | |
| | $S = 1$ | $S = 2$ | $S = 3$ | $S = 4$ |
| $L^{(S)}$ | 6.00 | 1.80 | 1.80 | 1.80 |
| $N^{(S)}$ | 100 | 208 | 208 | 208 |
| $Q^{(S)}$ | 100 | 144 | 36 | 36 |
| | $SNR = 10dB$ | | | |
| | $S = 1$ | $S = 2$ | $S = 3$ | $S = 4$ |
| $L^{(S)}$ | 6.00 | 1.80 | 1.80 | 1.80 |
| $N^{(S)}$ | 100 | 208 | 208 | 208 |
| $Q^{(S)}$ | 100 | 144 | 36 | 36 |
| | $SNR = 5dB$ | | | |
| | $S = 1$ | $S = 2$ | $S = 3$ | $S = 4$ |
| $L^{(S)}$ | 6.00 | 1.80 | 1.80 | 1.80 |
| $N^{(S)}$ | 100 | 208 | 208 | 208 |
| $Q^{(S)}$ | 100 | 144 | 36 | 36 |

Table VI: *L-shaped Object*, $\ell = 1.5\lambda$, $\tau = 0.10$ - Investigation domain parameters: restricted investigation domain size $L^{(S)}$, total number of cells $N^{(S)}$ and number of cells within the restricted domain size $Q^{(S)}$.

2.1.4 L-shaped Object, $\ell = 1.5\lambda$, $\tau = 0.15$ - IMSA-BCS reconstructed profiles

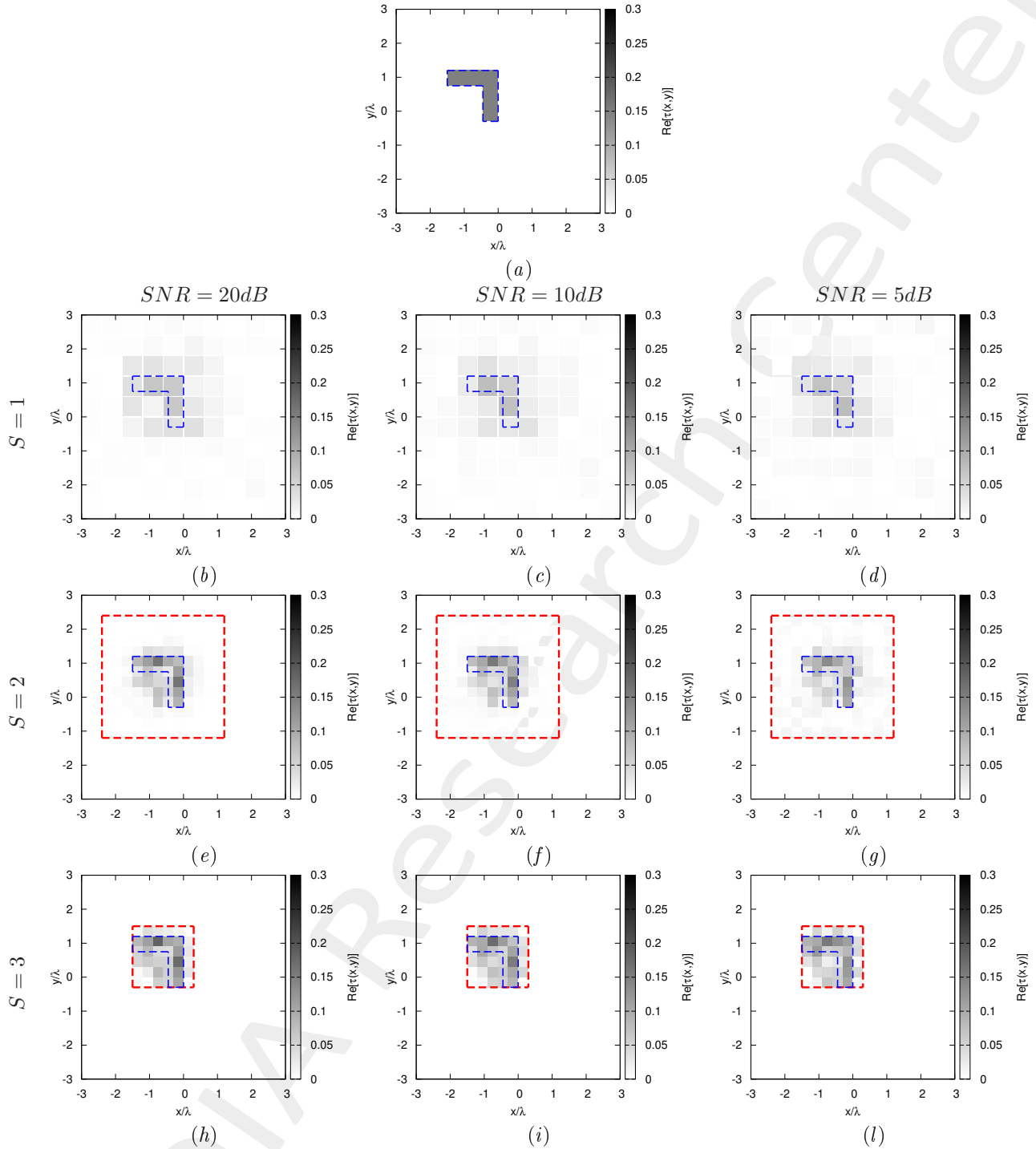


Figure 4: *L-shaped Object, $\ell = 1.5\lambda$, $\tau = 0.15$* - (a) Actual profile and (b)-(o) IMSA-BCS reconstructed profiles for (b)(e)(h) $SNR = 20 \text{ [dB]}$, (c)(f)(i) $SNR = 10 \text{ [dB]}$ and (d)(g)(l) $SNR = 5 \text{ [dB]}$ at the step (b)-(d) $S = 1$, (e)-(g) $S = 2$, and (h)-(l) $S = 3$.

| | $SNR = 50dB$ | | | |
|-------------|-----------------------|-----------------------|-----------------------|-----------------------|
| | $S = 1$ | $S = 2$ | $S = 3$ | $S = 4$ |
| ξ_{tot} | 8.88×10^{-3} | 4.04×10^{-3} | 3.48×10^{-3} | 3.48×10^{-3} |
| ξ_{int} | 8.11×10^{-2} | 5.20×10^{-2} | 4.62×10^{-2} | 4.62×10^{-2} |
| ξ_{ext} | 6.00×10^{-3} | 2.17×10^{-3} | 1.79×10^{-3} | 1.79×10^{-3} |
| | $SNR = 20dB$ | | | |
| | $S = 1$ | $S = 2$ | $S = 3$ | $S = 4$ |
| ξ_{tot} | 8.92×10^{-3} | 4.26×10^{-3} | 3.69×10^{-3} | 3.69×10^{-3} |
| ξ_{int} | 8.01×10^{-2} | 5.46×10^{-2} | 4.97×10^{-2} | 4.97×10^{-2} |
| ξ_{ext} | 5.97×10^{-3} | 2.33×10^{-3} | 1.92×10^{-3} | 1.92×10^{-3} |
| | $SNR = 10dB$ | | | |
| | $S = 1$ | $S = 2$ | $S = 3$ | $S = 4$ |
| ξ_{tot} | 9.16×10^{-3} | 4.68×10^{-3} | 3.87×10^{-3} | 3.87×10^{-3} |
| ξ_{int} | 8.02×10^{-2} | 5.41×10^{-2} | 5.03×10^{-2} | 5.03×10^{-2} |
| ξ_{ext} | 6.17×10^{-3} | 2.59×10^{-3} | 2.10×10^{-3} | 2.10×10^{-3} |
| | $SNR = 5dB$ | | | |
| | $S = 1$ | $S = 2$ | $S = 3$ | $S = 4$ |
| ξ_{tot} | 1.02×10^{-2} | 5.50×10^{-3} | 3.85×10^{-3} | 3.85×10^{-3} |
| ξ_{int} | 7.92×10^{-2} | 6.05×10^{-2} | 4.50×10^{-2} | 4.50×10^{-2} |
| ξ_{ext} | 6.81×10^{-3} | 3.12×10^{-3} | 2.06×10^{-3} | 2.06×10^{-3} |

Table VII: *L-shaped Object*, $\ell = 1.5\lambda$, $\tau = 0.10$ - Reconstruction errors: total (ξ_{tot}), internal (ξ_{int}) and external (ξ_{ext}) errors.

| | $SNR = 50dB$ | | | |
|-----------|--------------|---------|---------|---------|
| | $S = 1$ | $S = 2$ | $S = 3$ | $S = 4$ |
| $L^{(S)}$ | 6.00 | 1.80 | 1.80 | 1.80 |
| $N^{(S)}$ | 100 | 208 | 208 | 208 |
| $Q^{(S)}$ | 100 | 144 | 36 | 36 |
| | $SNR = 20dB$ | | | |
| | $S = 1$ | $S = 2$ | $S = 3$ | $S = 4$ |
| $L^{(S)}$ | 6.00 | 1.80 | 1.80 | 1.80 |
| $N^{(S)}$ | 100 | 208 | 208 | 208 |
| $Q^{(S)}$ | 100 | 144 | 36 | 36 |
| | $SNR = 10dB$ | | | |
| | $S = 1$ | $S = 2$ | $S = 3$ | $S = 4$ |
| $L^{(S)}$ | 6.00 | 1.80 | 1.80 | 1.80 |
| $N^{(S)}$ | 100 | 208 | 208 | 208 |
| $Q^{(S)}$ | 100 | 144 | 36 | 36 |
| | $SNR = 5dB$ | | | |
| | $S = 1$ | $S = 2$ | $S = 3$ | $S = 4$ |
| $L^{(S)}$ | 6.00 | 1.80 | 1.80 | 1.80 |
| $N^{(S)}$ | 100 | 208 | 208 | 208 |
| $Q^{(S)}$ | 100 | 144 | 36 | 36 |

Table VIII: *L-shaped Object*, $\ell = 1.5\lambda$, $\tau = 0.15$ - Investigation domain parameters: restricted investigation domain size $L^{(S)}$, total number of cells $N^{(S)}$ and number of cells within the restricted domain size $Q^{(S)}$.

2.1.5 L-shaped Object, $\ell = 1.5\lambda$, $\tau = 0.20$ - IMSA-BCS reconstructed profiles

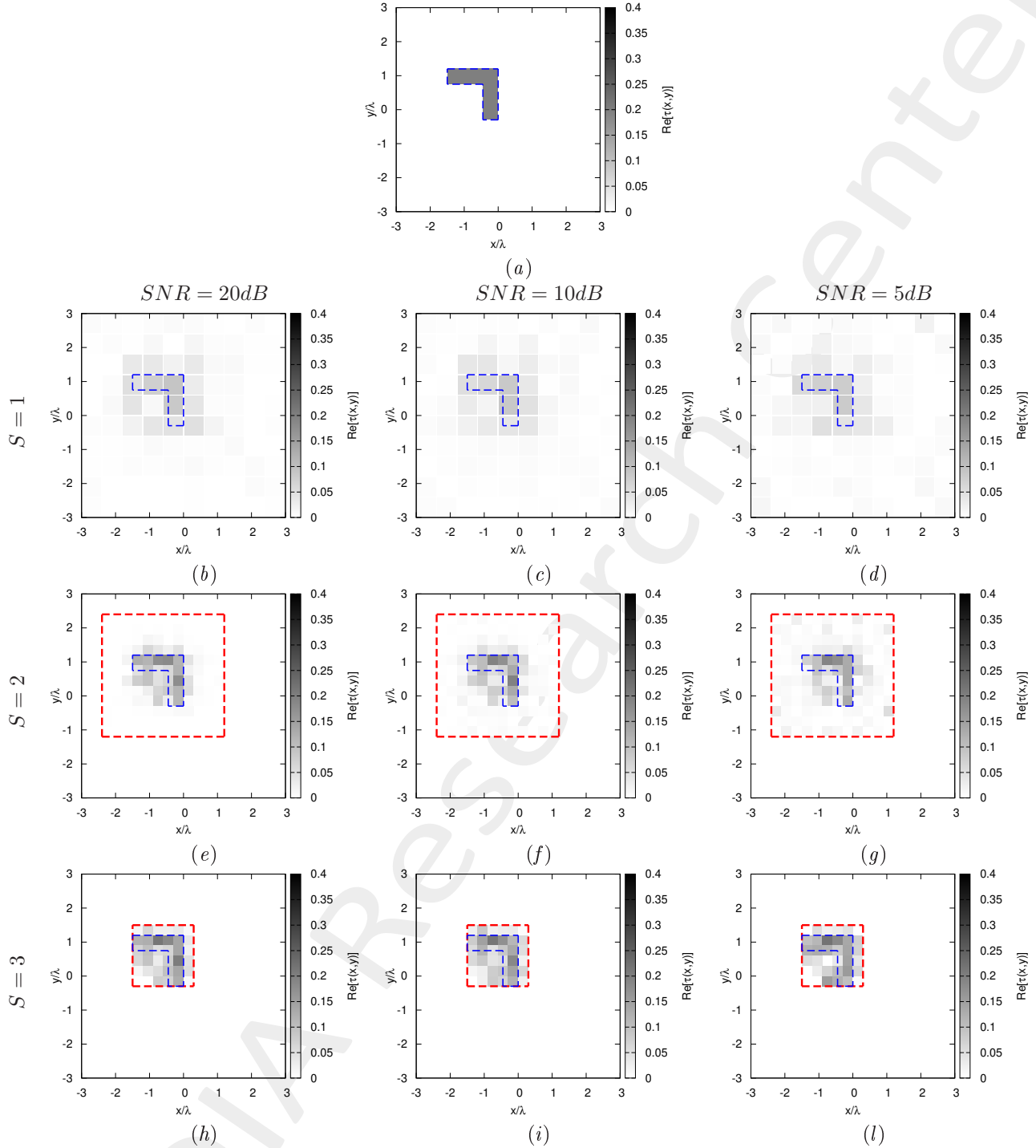


Figure 5: *L-shaped Object, $\ell = 1.5\lambda$, $\tau = 0.20$* - (a) Actual profile and (b)-(o) IMSA-BCS reconstructed profiles for (b)(e)(h) $SNR = 20$ [dB], (c)(f)(i) $SNR = 10$ [dB] and (d)(g)(l) $SNR = 5$ [dB] at the step (b)-(d) $S = 1$, (e)-(g) $S = 2$, and (h)-(l) $S = 3$.

| | $SNR = 50dB$ | | | |
|-------------|-----------------------|-----------------------|-----------------------|-----------------------|
| | $S = 1$ | $S = 2$ | $S = 3$ | $S = 4$ |
| ξ_{tot} | 1.21×10^{-2} | 6.02×10^{-3} | 4.90×10^{-3} | 4.90×10^{-3} |
| ξ_{int} | 1.07×10^{-1} | 7.30×10^{-2} | 5.81×10^{-2} | 5.81×10^{-2} |
| ξ_{ext} | 8.04×10^{-3} | 3.23×10^{-3} | 2.58×10^{-3} | 2.58×10^{-3} |
| | $SNR = 20dB$ | | | |
| | $S = 1$ | $S = 2$ | $S = 3$ | $S = 4$ |
| ξ_{tot} | 1.19×10^{-2} | 5.81×10^{-3} | 4.83×10^{-3} | 4.83×10^{-3} |
| ξ_{int} | 1.03×10^{-1} | 6.95×10^{-2} | 5.87×10^{-2} | 5.87×10^{-2} |
| ξ_{ext} | 7.98×10^{-3} | 3.13×10^{-3} | 2.51×10^{-3} | 2.51×10^{-3} |
| | $SNR = 10dB$ | | | |
| | $S = 1$ | $S = 2$ | $S = 3$ | $S = 4$ |
| ξ_{tot} | 1.27×10^{-2} | 6.40×10^{-3} | 5.23×10^{-3} | 5.23×10^{-3} |
| ξ_{int} | 1.07×10^{-1} | 7.19×10^{-2} | 6.41×10^{-2} | 6.41×10^{-2} |
| ξ_{ext} | 8.49×10^{-3} | 3.47×10^{-3} | 2.75×10^{-3} | 2.75×10^{-3} |
| | $SNR = 5dB$ | | | |
| | $S = 1$ | $S = 2$ | $S = 3$ | $S = 4$ |
| ξ_{tot} | 1.44×10^{-2} | 8.26×10^{-3} | 5.85×10^{-3} | 5.85×10^{-3} |
| ξ_{int} | 1.06×10^{-1} | 7.72×10^{-2} | 5.98×10^{-2} | 5.98×10^{-2} |
| ξ_{ext} | 9.55×10^{-3} | 4.70×10^{-3} | 3.09×10^{-3} | 3.09×10^{-3} |

Table IX: *L-shaped Object*, $\ell = 1.5\lambda$, $\tau = 0.20$ - Reconstruction errors: total (ξ_{tot}), internal (ξ_{int}) and external (ξ_{ext}) errors.

| | $SNR = 50dB$ | | | |
|-----------|--------------|---------|---------|---------|
| | $S = 1$ | $S = 2$ | $S = 3$ | $S = 4$ |
| $L^{(S)}$ | 6.00 | 1.80 | 1.80 | 1.80 |
| $N^{(S)}$ | 100 | 208 | 208 | 208 |
| $Q^{(S)}$ | 100 | 144 | 36 | 36 |
| | $SNR = 20dB$ | | | |
| | $S = 1$ | $S = 2$ | $S = 3$ | $S = 4$ |
| $L^{(S)}$ | 6.00 | 1.80 | 1.80 | 1.80 |
| $N^{(S)}$ | 100 | 208 | 208 | 208 |
| $Q^{(S)}$ | 100 | 144 | 36 | 36 |
| | $SNR = 10dB$ | | | |
| | $S = 1$ | $S = 2$ | $S = 3$ | $S = 4$ |
| $L^{(S)}$ | 6.00 | 1.80 | 1.80 | 1.80 |
| $N^{(S)}$ | 100 | 208 | 208 | 208 |
| $Q^{(S)}$ | 100 | 144 | 36 | 36 |
| | $SNR = 5dB$ | | | |
| | $S = 1$ | $S = 2$ | $S = 3$ | $S = 4$ |
| $L^{(S)}$ | 6.00 | 1.80 | 1.80 | 1.80 |
| $N^{(S)}$ | 100 | 208 | 208 | 208 |
| $Q^{(S)}$ | 100 | 144 | 36 | 36 |

Table X: *L-shaped Object*, $\ell = 1.5\lambda$, $\tau = 0.20$ - Investigation domain parameters: restricted investigation domain size $L^{(S)}$, total number of cells $N^{(S)}$ and number of cells within the restricted domain size $Q^{(S)}$.

2.1.6 L-shaped Object, $\ell = 1.5\lambda$, $\tau = 0.20$ - IMSA-BCS multi-resolution grids

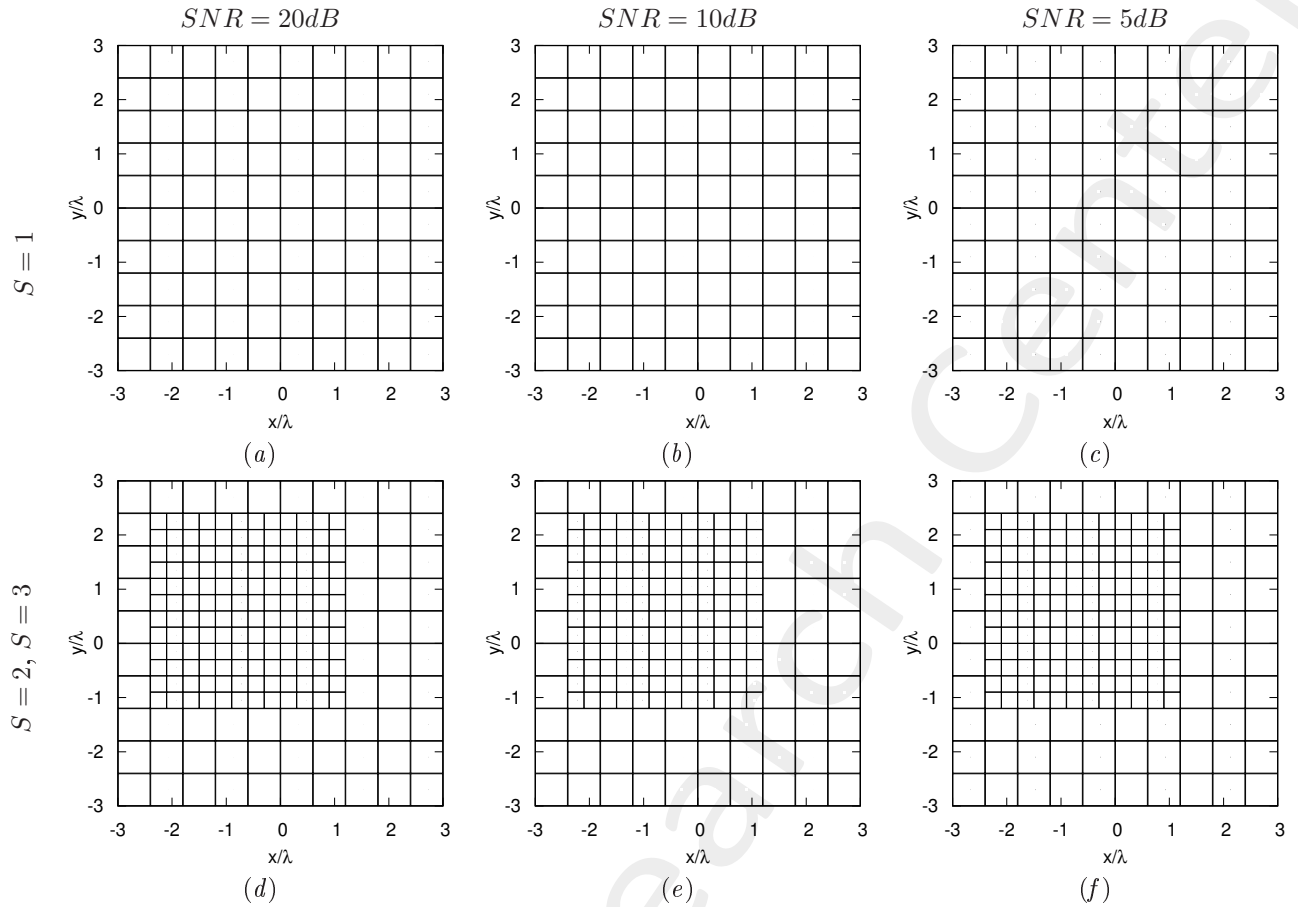


Figure 6: *L-shaped Object, $\ell = 1.5\lambda$, $\tau = 0.20$ - Example of IMSA-BCS multi-resolution grids for (a)-(d) $SNR = 20$ [dB], (b)-(e) $SNR = 10$ [dB] and (c)-(f) $SNR = 5$ [dB] at the step (a)-(c) $S = 1$ and (d)-(f) $S = 2, 3$.*

2.1.7 L-shaped Object, $\ell = 1.5\lambda$ - Resume: Errors vs. τ

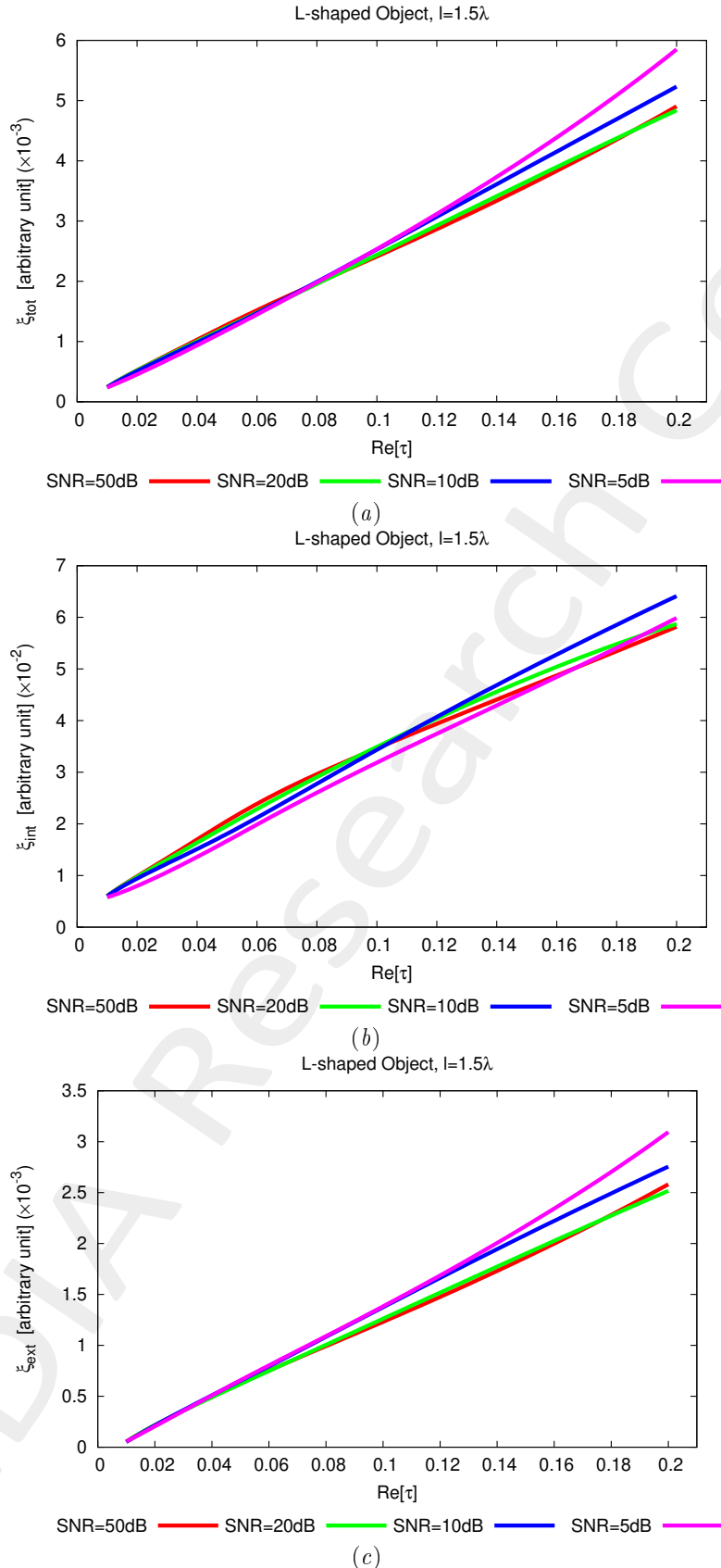


Figure 7: *L-shaped Object, $\ell = 1.5\lambda$ - Reconstruction errors vs. τ : (a) total error, (b) internal error and (c) external error.*

2.1.8 L-shaped Object, $\ell = 1.5\lambda$ - Resume: Errors vs. SNR

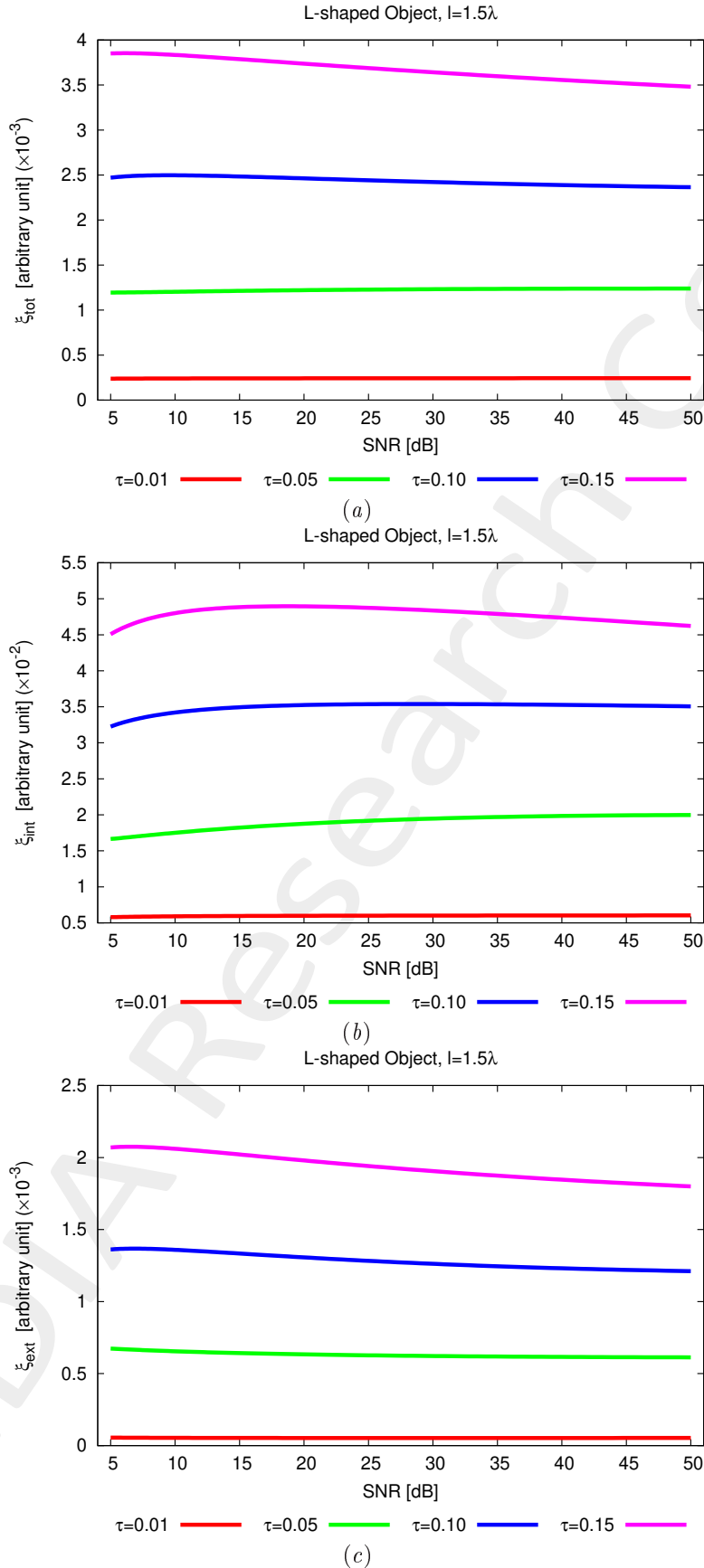


Figure 8: *L-shaped Object, $\ell = 1.5\lambda$* - Reconstruction errors vs. SNR: (a) total error, (b) internal error and (c) external error.

2.1.9 L-shaped Object, $\ell = 1.5\lambda$ - Resume: Errors vs. IMSA step, S

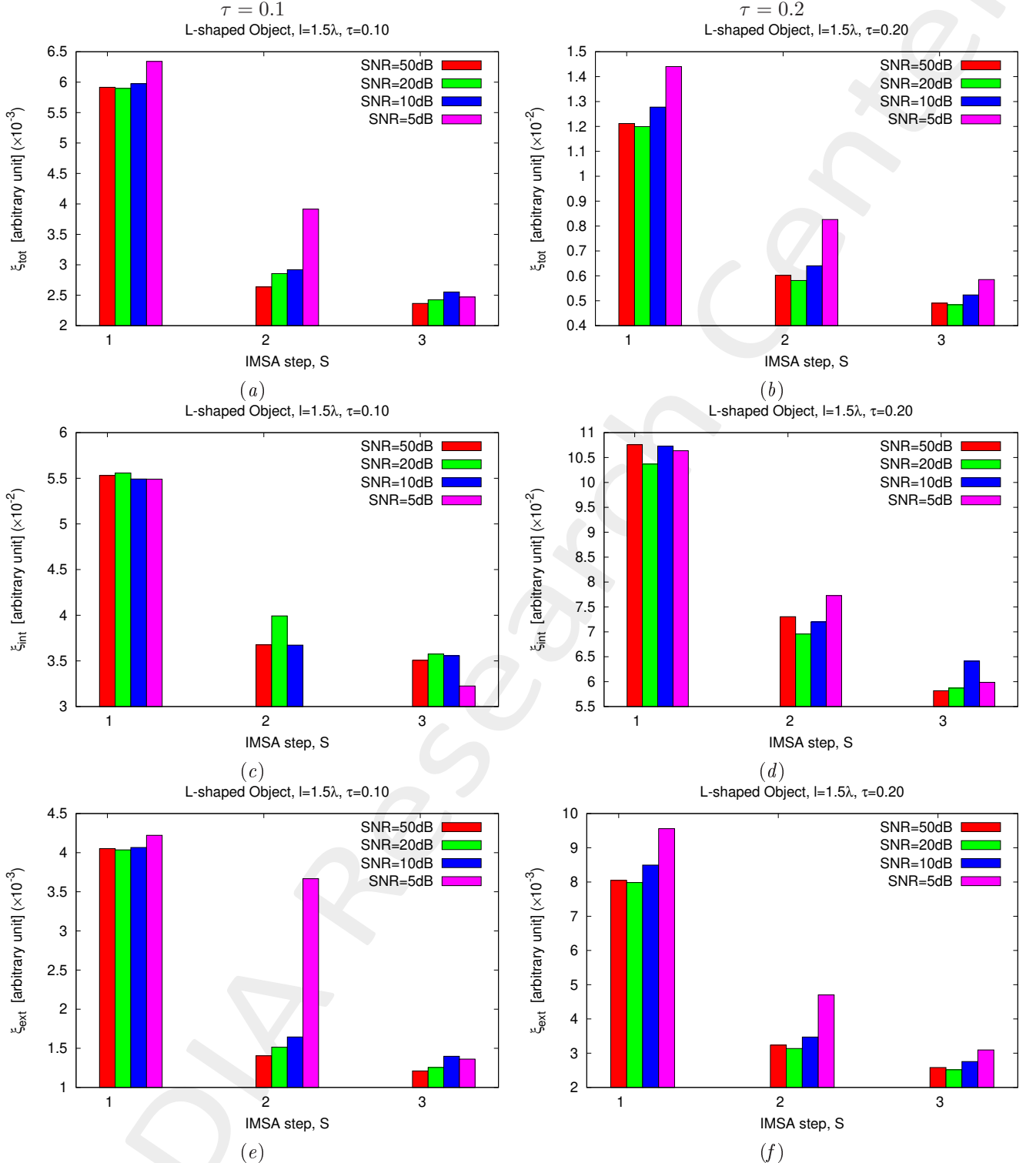


Figure 9: *L-shaped Object, $\ell = 1.5\lambda$ - Reconstruction errors vs. IMSA step, S :* (a)(b) total error, (c)(d) internal error and (e)(f) external error for (a)(c)(e) $\tau = 0.1$ and (b)(d)(f) $\tau = 0.2$.

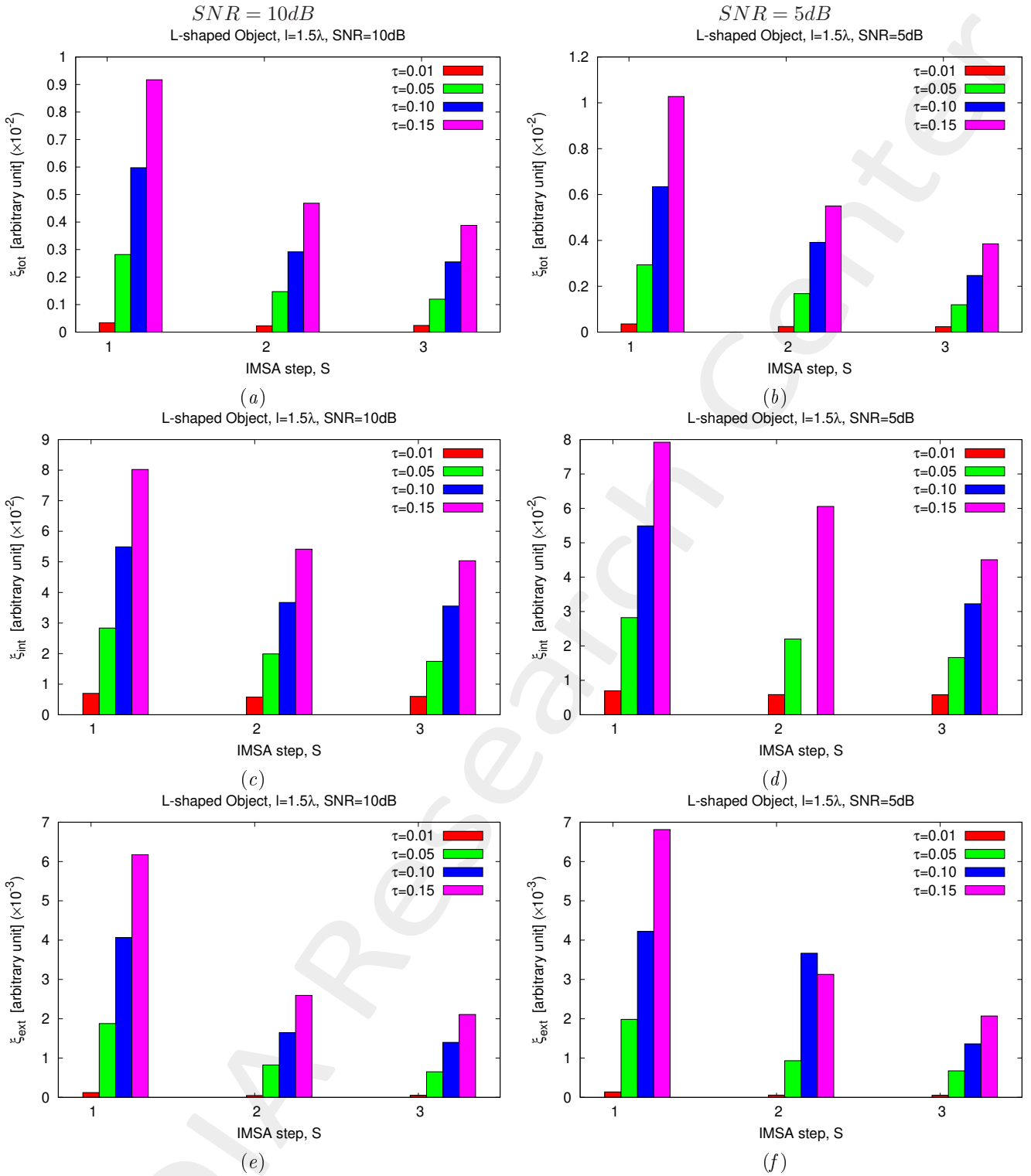


Figure 10: *L-shaped Object*, $\ell = 1.5\lambda$ - Reconstruction errors vs. *IMSA step, S*: (a)(b) total error, (c)(d) internal error and (e)(f) external error for (a)(c)(e) $SNR = 10dB$ and (b)(d)(f) $SNR = 5dB$.

More information on the topics of this document can be found in the following list of references.

References

- [1] M. Salucci, G. Oliveri, and A. Massa, "GPR prospecting through an inverse scattering frequency-hopping multi-focusing approach," *IEEE Trans. Geosci. Remote Sens.*, vol. 53, no. 12, pp. 6573-6592, Dec. 2015 (DOI: 10.1109/TGRS.2015.2444391).
- [2] M. Salucci, L. Poli, N. Anselmi, and A. Massa, "Multifrequency Particle Swarm Optimization for enhanced multi-resolution GPR microwave imaging," *IEEE Trans. Geosci. Remote Sens.*, vol. 55, no. 3, pp. 1305-1317, Mar. 2017 (DOI: 10.1109/TGRS.2016.2622061).
- [3] M. Salucci, L. Poli, and A. Massa, "Advanced multi-frequency GPR data processing for non-linear deterministic imaging," *Signal Processing - Special Issue on 'Advanced Ground-Penetrating Radar Signal-Processing Techniques,'* vol. 132, pp. 306-318, Mar. 2017 (DOI: 10.1016/j.sigpro.2016.06.019).
- [4] N. Anselmi, G. Oliveri, M. Salucci, and A. Massa, "Wavelet-based compressive imaging of sparse targets," *IEEE Trans. Antennas Propag.*, vol. 63, no. 11, pp. 4889-4900, Nov. 2015 (DOI: 10.1109/TAP.2015.2444423).
- [5] G. Oliveri, M. Salucci, N. Anselmi, and A. Massa, "Compressive sensing as applied to inverse problems for imaging: theory, applications, current trends, and open challenges," *IEEE Antennas Propag. Mag. - Special Issue on "Electromagnetic Inverse Problems for Sensing and Imaging,"* vol. 59, no. 5, pp. 34-46, Oct. 2017 (DOI: 10.1109/MAP.2017.2731204).
- [6] A. Massa, P. Rocca, and G. Oliveri, "Compressive sensing in electromagnetics - A review," *IEEE Antennas Propag. Mag.*, pp. 224-238, vol. 57, no. 1, Feb. 2015 (DOI: 10.1109/MAP.2015.2397092).
- [7] N. Anselmi, L. Poli, G. Oliveri, and A. Massa, "Iterative multi-resolution bayesian CS for microwave imaging," *IEEE Trans. Antennas Propag.*, vol. 66, no. 7, pp. 3665-3677, Jul. 2018 (DOI: 10.1109/TAP.2018.2826574).
- [8] N. Anselmi, G. Oliveri, M. A. Hannan, M. Salucci, and A. Massa, "Color compressive sensing imaging of arbitrary-shaped scatterers," *IEEE Trans. Microw. Theory Techn.*, vol. 65, no. 6, pp. 1986-1999, Jun. 2017 (DOI: 10.1109/TMTT.2016.2645570).
- [9] G. Oliveri, N. Anselmi, and A. Massa, "Compressive sensing imaging of non-sparse 2D scatterers by a total-variation approach within the Born approximation," *IEEE Trans. Antennas Propag.*, vol. 62, no. 10, pp. 5157-5170, Oct. 2014 (DOI: 10.1109/TAP.2014.2344673).
- [10] L. Poli, G. Oliveri, and A. Massa, "Imaging sparse metallic cylinders through a local shape function Bayesian compressive sensing approach," *J. Opt. Soc. Am. A*, vol. 30, no. 6, pp. 1261-1272, 2013 (DOI: 10.1364/JOSAA.30.001261).

-
- [11] L. Poli, G. Oliveri, F. Viani, and A. Massa, "MT-BCS-based microwave imaging approach through minimum-norm current expansion," *IEEE Trans. Antennas Propag.*, vol. 61, no. 9, pp. 4722-4732, Sep. 2013 (DOI: 10.1109/TAP.2013.2265254).
 - [12] F. Viani, L. Poli, G. Oliveri, F. Robol, and A. Massa, "Sparse scatterers imaging through approximated multitask compressive sensing strategies," *Microwave Opt. Technol. Lett.*, vol. 55, no. 7, pp. 1553-1558, Jul. 2013 (10.1002/mop.27612).
 - [13] L. Poli, G. Oliveri, P. Rocca, and A. Massa, "Bayesian compressive sensing approaches for the reconstruction of two-dimensional sparse scatterers under TE illumination," *IEEE Trans. Geosci. Remote Sens.*, vol. 51, no. 5, pp. 2920-2936, May 2013 (DOI: 10.1109/TGRS.2012.2218613).
 - [14] L. Poli, G. Oliveri, and A. Massa, "Microwave imaging within the first-order Born approximation by means of the contrast-field Bayesian compressive sensing," *IEEE Trans. Antennas Propag.*, vol. 60, no. 6, pp. 2865-2879, Jun. 2012 (DOI: 10.1109/TAP.2012.2194676).
 - [15] G. Oliveri, L. Poli, P. Rocca, and A. Massa, "Bayesian compressive optical imaging within the Rytov approximation," *Optics Letters*, vol. 37, no. 10, pp. 1760-1762, 2012 (DOI: 10.1364/OL.37.001760).
 - [16] G. Oliveri, P. Rocca, and A. Massa, "A Bayesian compressive sampling-based inversion for imaging sparse scatterers," *IEEE Trans. Geosci. Remote Sens.*, vol. 49, no. 10, pp. 3993-4006, Oct. 2011 (DOI: 10.1109/TGRS.2011.2128329).
 - [17] G. Oliveri, M. Salucci, and N. Anselmi, "Tomographic imaging of sparse low-contrast targets in harsh environments through matrix completion," *IEEE Trans. Microw. Theory Tech.*, vol. 66, no. 6, pp. 2714-2730, Jun. 2018 (DOI: 10.1109/TMTT.2018.2825393).
 - [18] M. Salucci, A. Gelmini, L. Poli, G. Oliveri, and A. Massa, "Progressive compressive sensing for exploiting frequency-diversity in GPR imaging," *J.Electromagn. Waves Appl.*, vol. 32, no. 9, pp. 1164-1193, 2018 (DOI: 10.1080/09205071.2018.1425160).